Enhanced reflection via phase compensation from anomalous dispersion in atomic vapor

Jun-Xiang Zhang,[1] Hai-Tao Zhou,[1] Da-Wei Wang,[2] and Shi-Yao Zhu[1,2,3]

[1]*The State Key Laboratory of Quantum Optics and Quantum Optics Devices, Institute of Opto-Electronics, Shanxi University, Taiyuan 030006, China*

[2]*Beijing Computational Science Research Center, Beijing 100084, China*

[3]*Department of Physics, Hong Kong Baptist University, Hong Kong, China*

(Received 6 October 2010; published 27 May 2011)

The phase compensation mechanism induced by anomalous dispersion in the reflection process of four-wave mixing (or reflection from a grating) in a three-level system is investigated, where the four wave vectors do not match in vacuum. An efficiency of the reflected signal of as high as 43% from a hot atomic cell of Cs is observed. The maximum reflection occurs when the frequency of the probe beam (and consequently the frequency of the reflected signal) is slightly red detuned from the transition frequency, which is attributed to the phase compensation from the steep anomalous dispersion accompanied with a strong probe absorption. The dependences of the efficiency on the angle between the coupling and probe lights, on the intensity of the coupling, field and on atomic density are studied. A theoretical model is presented and it is in good agreement with the experimental results.

DOI: 10.1103/PhysRevA.83.053841 PACS number(s): 42.50.Gy, 32.80.Wr, 42.50.Nn

I. INTRODUCTION

Quantum nonlinear dynamics is an important topic in physics. The optical nonlinearities such as four-wave parametric interaction [1] and parametric down conversion [2] can result in a large number of quantum effects, such as a squeezed state [1,2], all-optical switching [3], and quantum entanglement [4]. These effects are important for the research field of quantum information processing and communication [5]. Furthermore, the nonlinear process via atomic coherence has recently attracted much attention [6] due to its potential application in the storage of quantum information and quantum memory [7,8], cross-phase modulation [9], effective generation of squeezing without a cavity [10], multimode squeezing with possible applications to quantum imaging [11,12], and long-distance communication [13]. Experimental and theoretical studies have revealed that the atomic coherence generated by electromagnetically induced transparency (EIT) [14] plays an important role in the multiwave mixing process [15–19], as EIT modifies both absorptive and dispersive properties of an absorbing medium, which may lead to suppression of lower-order susceptibilities and the enhancement of higher-order susceptibilities by a slowly propagating wave.

In a three-level EIT system, the strong-coupling field is a traveling wave, and there is no absorption for the probe field. By using a standing wave for the coupling field in the three-level system, we obtain a narrow strong absorption with a steep anomalous dispersion [20–22] instead of transparency. At the same time of the probe absorption, a unique field is generated [23], which can be understood as the result of electromagnetically induced grating (EIG) due to spatially modulated absorption and dispersion (Bragg grating) [24]. The diffraction due to the Bragg grating generated by the standing wave has been observed in cold atoms [25–27]. When the probe is almost normal to the grating (almost parallel to the coupling field), the diffraction is usually called reflection [28], which was observed in hot atoms with and without a buffer gas [29–32]. This generation of a unique field can be explained also with a four-wave mixing (FWM) process [18]. In these studies [24–27,29–32], the frequency of the coupling field is smaller than the probe field frequency, so that the Bragg condition $2D = \lambda_c \geqslant \lambda_p$ can be satisfied for the probe, where λ_p and λ_c are the wavelength of the probe and the standing-wave coupling field, respectively, and D is the period of the grating; or the phase matching can be achieved for the four wave vectors of the related fields.

Here we report the experimental observation of 43% reflection efficiency of the probe with a probe frequency that is smaller than the frequency of the coupling standing wave, i.e., the Bragg condition cannot be fulfilled. Our theoretical analysis and experiment show that the high reflection is due to the strong anomalous dispersion, which results in the compensation to the phase mismatch.

II. EXPERIMENT

Consider the three-level system with one upper state $|a\rangle$ $(6^2P_{1/2}, F' = 4)$, and two ground states $|b\rangle$ $(6^2S_{1/2}, F = 4)$ and $|c\rangle$ $(6^2S_{1/2}, F = 3)$ of the ^{133}Cs D_1 line; see Fig. 1(a). The transition frequencies from $|a\rangle$ to $|c\rangle$ and $|b\rangle$ are ω_{ac} and ω_{ab}, respectively, with $\omega_{ac} = \omega_{ab} + 2\pi \times 9.2$ GHz. The decay rate of the upper state to the ground states is $\Gamma_a = 2\pi \times 4.6$ MHz. Two strong copropagating and counterpropagating coupling fields with frequency $\omega_c = \omega_{ac}$ propagate in the x direction, and drive the transition between $|a\rangle$ and $|c\rangle$, a weak probe light (ω_p) scanning across the transition of $|a\rangle$ and $|b\rangle$ is incident with a small angle θ into the cell, see Fig. 1(b). In this experiment, the frequency of the coupling field is larger than that of the probe field, $\omega_c > \omega_p$, which violates the geometric Bragg condition $\omega_c/\omega_p = \cos\theta$. In other words, the vacuum wave vectors of the driving fields, probe field, and the reflected field do not meet the phase-matching condition. The Cs vapor cell with antireflection-coated end windows (the loss of the far-off resonant light through the cell is measured to be 4%) has a length $L = 7.5$ cm; the temperature (T) is controlled from 28 °C to 82 °C, which corresponds to an atom density of $0.07–4.52 \times 10^{18}$ m^{-3}. The power of the copropagating coupling field is 20 mW with an e^{-2} full width of 0.64 mm,

 ©2011 American Physical Society

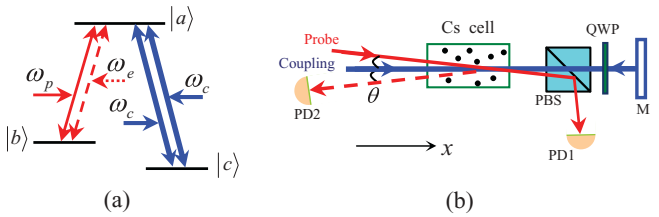

FIG. 1. (Color online) (a) Λ-type three-level scheme. (b) Experimental setup. PBS: polarizing beam splitter; QWP: quarter-wave plate; M: reflection-mirror; PD1,2: photodetectors.

and the counterpropagating coupling field is formed from the reflected copropagating coupling field via a quarter-wave plate and a reflection mirror M; its power is varied by the reflection coefficient R. The power of the probe is 90 μW (only 0.45% of the coupling power) with an e^{-2} full width of 0.59 mm.

In Fig. 2(a), we plot the absorption coefficient $\alpha = L^{-1}\ln(P_{\rm in}/P_{\rm out})$ vs $\Delta_p = \omega_p - \omega_{ab}$ for different R. $P_{\rm in}$ and $P_{\rm out}$ are the input and output powers of the probe light, respectively. For $R=0$, the EIT spectrum is observed [see the cyan curve (1)], and for $R=1$, a narrow absorption peak is observed [see the black curve (5)]. From $R=0$ to $R=1$, we see the gradual transformation of the EIT dip into a narrow absorption peak, with small dips at the middle of curves (2), (3), and (4). For $R \neq 1$, the coupling field can be approximately considered to be composed of two parts, a standing wave and a forward (copropagation) field that results in a EIT dip (residual EIT), which is true even for $R=1$ because of various losses. To measure the dispersion properties of the medium, we use the homodyne method based on a Mach-Zehnder interferometer to detect the phase shift $\Delta\Phi$ of the probe light passing through the cell. Figure 2(b) shows the $\Delta\Phi$ as a function of Δ_p. From EIT to the narrow absorption peak, the dispersion is changed gradually from a normal [curve (1)] to a steep anomalous dispersion [curve (5)]. The small normal dispersion region at zero detuning is due to the residual EIT.

Once the counterpropagating coupling field is turned on, the emission signal with frequency $\omega_r \approx \omega_p$ at the reflection direction from the vapor cell is detected by detector PD2 [see Fig. 1(b)]. We measure the reflection efficiency $\eta = P_r/P_{\rm in}$ (reflected field power P_r over the input probe power) versus probe detuning at different angles (see Fig. 3), and as high as 11% efficiency is observed at $\theta = 0.14^\circ$ and $T=43\,^\circ$C [curve (1)]. The larger measurement angle leads to a decrease of the reflection efficiency [see curves (1)–(4)]. Although not shown in Fig. 3, the saturation absorption spectrum of the probe light is simultaneously recorded to monitor the frequency of the

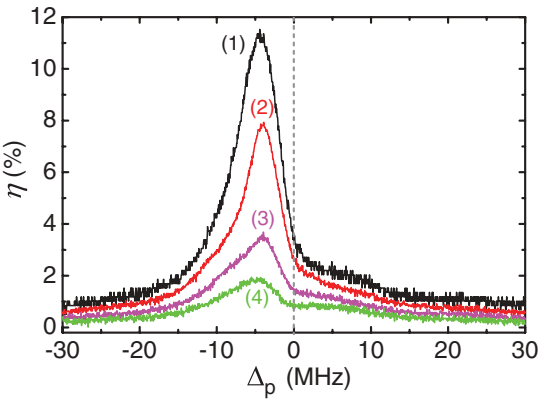

FIG. 3. (Color online) The reflection efficiency vs probe detuning for different angles at $T = 43\,^\circ$C. Curve (1) (black line): $\theta = 0.14\,^\circ$; curve (2) (red line): $\theta = 0.24^\circ$; curve (3) (magenta line): $\theta = 0.34\,^\circ$; and curve (4) (green line): $\theta = 0.44\,^\circ$. The other parameters are the same as those in Fig. 2.

reflected signal, and it is noted that the peaks of the reflection spectrum are red-detuned from an atomic transition of ~5 MHz when the system is driven by a resonant standing-wave field. The smaller the angle is, the higher is the efficiency. A maximum efficiency could be observed at $\theta = 0^\circ$, but in the case of $\theta = 0^\circ$, the beam of the reflected signal overlaps that of the input probe, and it is not possible to collect the complete reflected signal.

The reflection efficiency also strongly depends on the power of the coupling field, the temperature of the atoms, or the number density of the atoms. When the power of the coupling standing wave P_s (for $P_s = P_{c1} = P_{c2}$, P_{c1} and P_{c2} represent the power of forward and backward coupling field) increases, the efficiency increases from few percent to 12% at $T=43\,^\circ$C [see the black dots in Fig. 4(a)], and the saturation reaches $P_s = 20$ mW. If we fix the power of the copropagating coupling field ($P_{c1} = 20$ mW) and increase the power of the counterpropagating coupling field P_{c2} via changing R from 0 to 1 (from a traveling coupling field to a complete standing-wave coupling field), the efficiency still increases with increasing P_{c2} [see the red triangle dots in Fig. 4(a)]. A comparison between the two curves in Fig. 4(a) shows us that without complete standing-wave coupling, we still have significant reflection, but the efficiency is smaller for the case of a complete standing-wave coupling field, which means that the stronger absorption of the probe with steeper anomalous dispersion (see Fig. 2) gives a higher reflection efficiency. When the temperature increases from 35 °C to 80 °C, as high

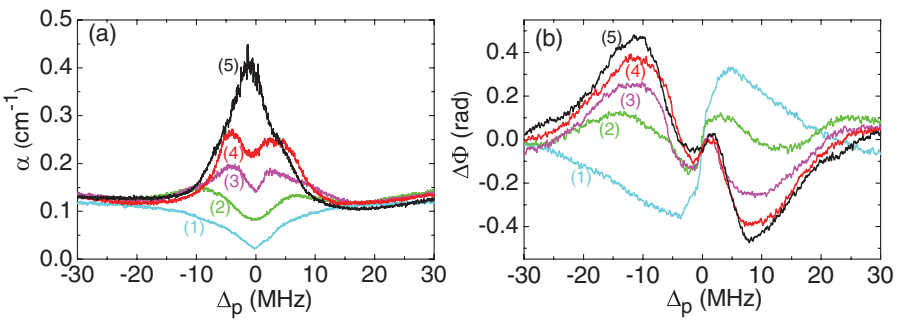

FIG. 2. (Color online) Measured transmission (a) and phase shift (b) of probe light vs probe detuning Δ_p for different R: (1) $R=0$ (cyan line); (2) $R=0.25$ (green line); (3) $R=0.5$ (magenta line); (4) $R=0.75$ (red line); and (5) $R=1$ (black line). The other parameters are $\theta = 0.14^\circ$ and $T = 28\,^\circ$C.

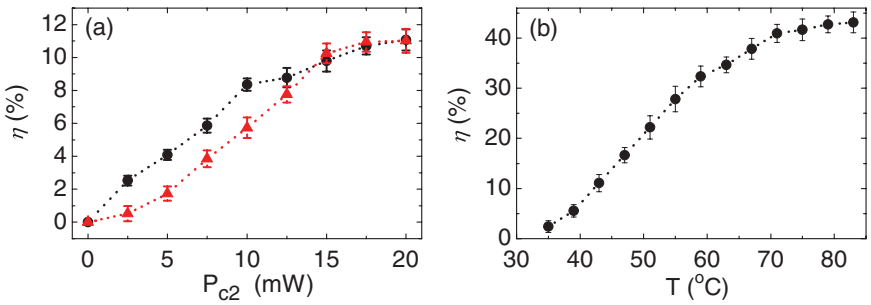

FIG. 4. (Color online) The efficiency vs the coupling power for $R=1$ and different R (a), and the cell temperature with $R=1$ (b). The other parameters are the same as those in Fig. 2.

as 43% efficiency is observed (with angle $\theta = 0.14^\circ$ and $R=1$) due to the increase in atom density. Saturation reaches at 80 °C [see Fig. 4(b)].

What is the physics behind the measurement results where the geometric Bragg condition is violated and the phase matching for the vacuum wave vectors is not met? Furthermore, the atomic velocity distribution (at above room temperature) makes the periodical structure very weak. From Figs. 2 and 4, we know that high reflection occurs in the atomic system with strong probe absorption and large anomalous dispersion (phase shift) for the probe light. Therefore, we need to consider the absorption (and dispersion) and emission by all the atoms in the cell with different velocities, which come from the atomic dipole between $|a\rangle$ and $|b\rangle$.

III. THEORY

Now we turn to the theoretical interpretation of the reflection process. Consider the three-level atom in Fig. 1(a) in the frame moving with the atom, which is coupled to two counterpropagating coupling fields $E_{c1,c2}(z,t) = \frac{1}{2}E_{c1,c2}e^{i(\vec{k}_{c1,c2}\cdot\vec{r}-\omega_{c1,c2}t)} + \text{c.c.}$ with frequency ω_{c1}, ω_{c2} and wave vectors $\vec{k}_{c1}$, $\vec{k}_{c2}$, and one weak probe field $E_p(z,t) = \frac{1}{2}E_p e^{i(\vec{k}_p\cdot\vec{r}-\omega_p t)} + \text{c.c.}$ with frequency ω_p and wave vector $\vec{k}_p$. The time evolutions of the density-matrix elements are

$$\dot{\rho}_{ab} = (-i\omega_{ab} - \Gamma_a/2)\rho_{ab} - i\Omega_p e^{-i\omega_p t}(\rho_{aa}-\rho_{bb}) + i(\Omega_{c1}e^{-i\omega_{c1}t} + \Omega_{c2}e^{-i\omega_{c2}t})\rho_{cb}, \tag{1a}$$

$$\dot{\rho}_{cb} = (-i\omega_{cb} - \gamma_{cb})\rho_{cb} - i\Omega_p e^{-i\omega_p t}\rho_{ca} + i(\Omega_{c1}^* e^{i\omega_{c1}t} + \Omega_{c2}^* e^{i\omega_{c2}t})\rho_{ab}, \tag{1b}$$

$$\dot{\rho}_{ca} = (-i\omega_{ca} - \Gamma_a/2)\rho_{ca} - i\Omega_p^* e^{i\omega_p t}\rho_{cb} + i(\Omega_{c1}^* e^{i\omega_{c1}t} + \Omega_{c2}^* e^{i\omega_{c2}t})(\rho_{aa}-\rho_{cc}), \tag{1c}$$

$$\dot{\rho}_{bb} = \gamma_{ab}\rho_{aa} - i\Omega_p e^{-i\omega_p t}\rho_{ba} + i\Omega_p^* e^{i\omega_p t}\rho_{ab}, \tag{1d}$$

$$\dot{\rho}_{cc} = \gamma_{ca}\rho_{aa} - i(\Omega_{c1}e^{-i\omega_1 t} + \Omega_{c2}e^{-i\omega_2 t})\rho_{ca} + i(\Omega_{c1}^* e^{i\omega_{c1}t} + \Omega_{c2}^* e^{i\omega_{c2}t})\rho_{ac}, \tag{1e}$$

$$\rho_{aa} + \rho_{bb} + \rho_{cc} = 1, \tag{1f}$$

where $\Omega_{c1} = \frac{\mu_{ac}E_{c1}}{2\hbar}$,$\Omega_{c2} = \frac{\mu_{ac}E_{c2}}{2\hbar}$,$\Omega_p = \frac{\mu_{ab}E_p}{2\hbar}$ are the Rabi frequencies of copropagating and counterpropagating coupling and probe fields, and μ_{ij} is the relevant dipole moment of transition $|i\rangle \leftrightarrow |j\rangle$. $\Gamma_a/2$ is the decoherence rate between the excited state $|a\rangle$ and the ground states $|b\rangle$, $|c\rangle$, respectively. γ_{cb} is the dephasing rate between two ground states. Note that the wave vectors of the two coupling fields are in opposite directions, $\vec{k}_{c1} = -\vec{k}_{c2} = \vec{k}_c$, and the frequencies have a difference $\omega_{c2} - \omega_{c1} = \delta$ due to the atomic velocity. The atom moving with velocity v in the direction of x "sees" the frequencies of the probe and the copropagating coupling beams are shifted by an amount of $-\omega_p v/c$ and $-\omega_{c1}v/c$, respectively, and the frequency of the counterpropagating coupling beam is shifted by $\omega_{c2}v/c$.

Because the probe field is much weaker than the coupling field, the atoms mostly populate the ground state $|b\rangle$. We perform a rotating-frame transformation using $\rho_{ab} = \tilde{\rho}_{ab}e^{-i\omega_p t}$, $\rho_{ac} = \tilde{\rho}_{ac}e^{-i\omega_{c1}t}$, $\rho_{cb} = \tilde{\rho}_{cb}e^{-i(\omega_p-\omega_{c1})t}$. The solution of Eqs. (1) can be solved in the form

$$\tilde{\rho}_{ij} = \sum_n \tilde{\rho}_{ij}^{[n]} e^{-in\delta t} \quad (n = 0, \pm 1, \ldots), \tag{2}$$

where $\tilde{\rho}_{ij}^{[n]}$ is the Fourier component of $\tilde{\rho}_{ij}$, which is related to important physical properties we will discuss later. By keeping to the first order of the probe field Rabi frequency Ω_p and all orders of the Rabi frequencies of coupling fields $\Omega_{c1,c2}$, we obtain

$$\tilde{\rho}_{ab}^{[n]} = \frac{-i\Omega_p\delta_{n,0} - i\Omega_{c1}\tilde{\rho}_{cb}^{[n]} - i\Omega_{c2}\tilde{\rho}_{cb}^{[n-1]}}{i\Delta_p - \gamma_{ab} + in\delta}, \tag{3a}$$

$$\tilde{\rho}_{cb}^{[n]} = \frac{-i\Omega_{c1}^*\tilde{\rho}_{ab}^{[n]} - i\Omega_{c2}^*\tilde{\rho}_{ab}^{[n+1]}}{i(\Delta_p - \Delta_{c1}) - \gamma_{cb} + in\delta}, \tag{3b}$$

where $\Delta_p = \omega_p - \omega_{ab}$ and $\Delta_{c1} = \omega_{c1} - \omega_{ac}$ are the detunings of the probe and copropagating coupling lights, respectively. In Eq. (3a), $\tilde{\rho}_{ab}^{[0]}$ is the synchronic frequency coherence of the probe light (it determines the linear absorption and dispersion properties of probe light), and $\tilde{\rho}_{ab}^{[n]}$ ($n \geqslant 1$) are the difference frequency coherences, which result in the nonlinear process. The absolute value of the square of $\tilde{\rho}_{ab}^{[n]}$ is related to the intensity of the generated signal with frequency $\omega_e = \omega_p + n\delta$ via a nonlinear process, and is strongly correlated to the ground-state atomic coherence $\tilde{\rho}_{cb}^{[n]}$. On the other hand, $\tilde{\rho}_{cb}^{[n]}$ is directly determined by the Rabi frequency of the coupling fields $\Omega_{c1,c2}$; it is very large at the two-photon resonance [$\Delta_p - \Delta_{c1} = 0$ in Eq. (3b)] between the copropagating coupling and probe lights. Especially for $n=1$, the generated signal results from both the zero-order ground-state coherence $\tilde{\rho}_{cb}^{[0]}$ and the counterpropagating coupling field [see the second term in Eq. (4a)], and it is enhanced by the higher-order ground-state coherence $\tilde{\rho}_{cb}^{[1]}$, which in turn is induced by the first and second

order of $\tilde{\rho}_{ab}^{[n]}$ [see Eq. (4b)]. For $n=1$, the process is described as a FWM:

$$\tilde{\rho}_{ab}^{[1]} = \frac{-i\Omega_{c1}\tilde{\rho}_{cb}^{[1]} - i\Omega_{c2}\tilde{\rho}_{cb}^{[0]}}{i\Delta_p - \gamma_{ab} + i\delta}, \tag{4a}$$

$$\tilde{\rho}_{cb}^{[1]} = \frac{-i\Omega_{c1}^{*}\tilde{\rho}_{ab}^{[1]} - i\Omega_{c2}^{*}\tilde{\rho}_{ab}^{[2]}}{i(\Delta_p - \Delta_{c1}) - \gamma_{cb} + i\delta}, \tag{4b}$$

$$\tilde{\rho}_{cb}^{[0]} = \frac{-i\Omega_{c1}^{*}\tilde{\rho}_{ab}^{[0]} - i\Omega_{c2}^{*}\tilde{\rho}_{ab}^{[1]}}{i(\Delta_p - \Delta_{c1}) - \gamma_{cb}}. \tag{4c}$$

The solution of $\tilde{\rho}_{ab}^{[n]}$ is obtained from the recursion relation

$$\tilde{\rho}_{ab}^{[n]} = P_n^{-1}\Bigg(-\Omega_p\delta_{n,0} + \frac{\Omega_{c1}^{*}\Omega_{c2}}{(\Delta_p - \Delta_{c2}) + n\delta + i\gamma_{cb}}\tilde{\rho}_{ab}^{[n-1]} + \frac{\Omega_{c1}\Omega_{c2}^{*}}{(\Delta_p - \Delta_{c1}) + n\delta + i\gamma_{cb}}\tilde{\rho}_{ab}^{[n+1]}\Bigg), \tag{5}$$

where

$$P_n = (\Delta_p + n\delta + i\gamma_{ab}) - \Bigg(\frac{|\Omega_{c1}|^2}{(\Delta_p - \Delta_{c1}) + n\delta + i\gamma_{cb}} + \frac{|\Omega_{c2}|^2}{(\Delta_p - \Delta_{c2}) + n\delta + i\gamma_{cb}}\Bigg).$$

Introducing the ratio $Z_n = \tilde{\rho}_{ab}^{[n]}/\tilde{\rho}_{ab}^{[n-1]}$ for $n \neq 0$, we get

$$Z_n = \frac{\Omega_{c1}^{*}\Omega_{c2}U_n}{1 - \frac{|\Omega_{c1}|^2|\Omega_{c2}|^2T_n}{1-\cdots}} \quad (n = \pm 1, \ldots), \tag{6}$$

where

$$U_n = \frac{1}{P_n[(\Delta_p - \Delta_{c2}) + n\delta + i\gamma_{cb}]},$$

$$T_n = \frac{U_{n+1}}{P_n[(\Delta_p - \Delta_{c1}) + n\delta + i\gamma_{cb}]}.$$

We obtain finally

$$\tilde{\rho}_{ab}^{[0]} = \frac{-\Omega_p}{P_0 - \frac{\Omega_{c1}\Omega_{c2}^{*}Z_1}{(\Delta_p - \Delta_{c1}) + i\gamma_{cb}} - \frac{\Omega_{c1}^{*}\Omega_{c2}X_1}{(\Delta_p - \Delta_{c2}) + i\gamma_{cb}}}, \tag{7a}$$

$$\tilde{\rho}_{ab}^{[1]} = \frac{-\Omega_p\Omega_{c1}^{*}\Omega_{c2}}{P_0 - \frac{\Omega_{c1}\Omega_{c2}^{*}Z_1}{(\Delta_p - \Delta_{c1}) + i\gamma_{cb}} - \frac{\Omega_{c1}^{*}\Omega_{c2}X_1}{(\Delta_p - \Delta_{c2}) + i\gamma_{cb}}} \frac{U_1}{1 - \frac{|\Omega_{c1}|^2|\Omega_{c2}|^2T_1}{1-\cdots}}, \tag{7b}$$

$$\tilde{\rho}_{ab}^{[2]} = \frac{-\Omega_p\Omega_{c1}^{*}\Omega_{c2}\Omega_{c1}^{*}\Omega_{c2}}{P_0 - \frac{\Omega_{c1}\Omega_{c2}^{*}Z_1}{(\Delta_p - \Delta_{c1}) + i\gamma_{cb}} - \frac{\Omega_{c1}^{*}\Omega_{c2}X_1}{(\Delta_p - \Delta_{c2}) + i\gamma_{cb}}} \frac{U_1}{1 - \frac{|\Omega_{c1}|^2|\Omega_{c2}|^2T_1}{1-\cdots}} \times \frac{U_2}{1 - \frac{|\Omega_{c1}|^2|\Omega_{c2}|^2T_2}{1-\cdots}}, \tag{7c}$$

where

$$X_1 = \frac{\Omega_{c1}\Omega_{c2}^{*}K_1}{1 - \frac{|\Omega_{c1}|^2|\Omega_{c2}|^2L_1}{1-\cdots}},$$

with

$$K_n = \frac{1}{P_{-n}[(\Delta_p - \Delta_{c1}) - n\delta + i\gamma_{cb}]},$$

$$L_n = \frac{K_{n+1}}{P_{-n}[(\Delta_p - \Delta_{c2}) - n\delta + i\gamma_{cb}]}.$$

The real and imaginary parts of χ correspond to the dispersion and the absorption of the probe field, respectively, and are related to $\tilde{\rho}_{ab}^{[0]}$ by the polarization relation $P = \frac{1}{2}\varepsilon_0\chi E_p e^{-i\omega_p t} + \text{c.c.} = \mu_{ab}N\tilde{\rho}_{ab}^{[0]}e^{-i\omega_p t} + \text{c.c.}$, where ε_0 is the free-space permittivity, and N is the atom number density. In this system of gas atoms, the influence of Doppler broadening has to be taken into account. Considering all the atoms in the vapor cell, we need to take an integration over the velocity distribution $f(v) = \sqrt{\frac{m}{2\pi k_B T}}\exp(-\frac{mv^2}{2k_B T})$, where $\sqrt{\frac{2k_B T}{m}}$ is the most probable speed of atoms at a given temperature T, m is the atomic mass, and k_B is the Boltzmann constant. We make the average over all Doppler detuning by replacing the detuning $\Delta_{c1} \to \Delta_{c1} - (\omega_{c1}v/c)$, $\Delta_p \to \Delta_p - (\omega_p v/c)$, and $\Delta_{c2} \to \Delta_{c2} + (\omega_{c2}v/c)$ for different velocities in the laboratory frame, and get the total susceptibility

$$\chi = \int_{-\infty}^{+\infty} \frac{(-N|\mu_{ab}|^2/\varepsilon_0\hbar)\sqrt{\frac{m}{2\pi k_B T}}\exp\left(-\frac{mv^2}{2k_B T}\right)}{\left(\Delta_p - \frac{\omega_p v}{c} + i\gamma_{ab}\right) - \frac{\Omega_{c1}(\Omega_{c1}^{*} + \Omega_{c2}^{*}Z_1)}{(\Delta_p - \Delta_{c1}) + \frac{(\omega_{c1} - \omega_p)v}{c} + i\gamma_{cb}} - \frac{\Omega_{c2}(\Omega_{c2}^{*} + \Omega_{c1}^{*}X_1)}{(\Delta_p - \Delta_{c2}) - \frac{(\omega_p + \omega_{c2})v}{c} + i\gamma_{cb}}} dv. \tag{8}$$

The imaginary and real parts of Eq. (8) for different ratios of the Rabi frequency ($R = |\Omega_{c2}|^2/|\Omega_{c1}|^2$) are plotted in Figs. 5(a) and 5(b), which are in good agreement with the experimental observation [Figs. 2(a) and 2(b)]. A minor discrepancy exists between theory and the experiment for curve (5) in Figs. 2(b) and 5(b), since the Rabi frequencies of the forward and backward coupling fields are not exactly the same in the experiment because of the loss from optics for the backward coupling field.

It can be proved easily from Eq. (7) that the generated signal is proportional to $\tilde{\rho}_{ab}^{[n]} \propto \Omega_p(\Omega_{c1}^{*}\Omega_{c2})^n \propto \exp\{i[\vec{k}_p - \vec{k}_r - n(\vec{k}_{c1} - \vec{k}_{c2})]\cdot\vec{r}\}$ with the wave vector $\vec{k}_r$. Note that the wave vectors of the coupling beams are set $\vec{k}_{c1} = -\vec{k}_{c2} = \vec{k}_c$ in the discussed configuration. So the nth-order generated signal $n \neq 0$ from different velocity atoms is small due to a large phase mismatch except for $n = 1$. For $n = 1$, the generated signal $\rho_{ab}^{[1]} \propto \Omega_p\Omega_{c1}^{*}\Omega_{c2} \propto \exp[i(\vec{k}_p - \vec{k}_r - 2\vec{k}_c)\cdot\vec{r}]$ is

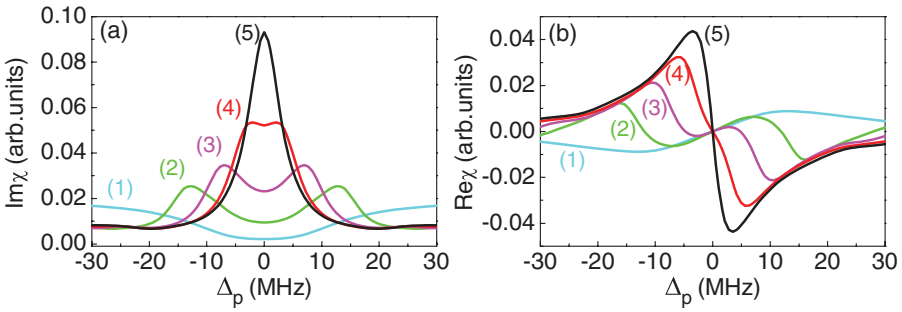

FIG. 5. (Color online) The absorption (a) and dispersion (b) of probe light vs probe detuning Δ_p for different ratio of Rabi frequency $R = \Omega_{c2}^2/\Omega_{c1}^2$. Curve (1): $R = 0$ (cyan line); curve (2): $R = 0.25$ (green line); curve (3): $R = 0.5$ (magenta line); curve (4): $R = 0.75$ (red line); and curve (5): $R = 1$ (black line). The parameters are $\gamma_{ab} = 0.5\Gamma_a$, $\gamma_{cb} = 0.03\Gamma_a$, $\Omega_p = 2\pi \times 3$ MHz, $\Omega_{c1} = 2\pi \times 50$ MHz, and the density of atoms is $10^{15}/\mathrm{m}^3$.

relatively large because the phase roughly matches $\Delta\vec{k} = \vec{k}_p - \vec{k}_r - 2\vec{k}_c \approx 0$.

Field $\vec{E}_r$ reflected by the atoms along the direction of $\vec{k}_r$ is

$$\vec{E}_r(\vec{r},t) \propto \sum_i \tilde{\rho}_{ab}^{[1]} e^{i(\vec{k}_p - \vec{k}_r - 2\vec{k}_c)\cdot\vec{r}_i} e^{-i\omega_r t}, \tag{9}$$

where the summation is over all the atoms. The total intensity of the output reflected signal off the vapor cell (the length L) is

$$I_r = \frac{c}{2\pi}|\vec{E}_r(\vec{r},t)|^2 \propto |\Omega_p\Omega_{c1}\Omega_{c2}|^2 |f^{[1]}(\Omega_{c1},\Omega_{c2})|^2 \times \frac{\sin^2\left(\frac{\Delta kL}{2}\right)}{\left(\frac{\Delta kL}{2}\right)^2}, \tag{10}$$

with

$$f^{[1]}(\Omega_{c1},\Omega_{c2}) = \frac{1}{P_0 - \frac{\Omega_{c1}\Omega_{c2}^* Z_1}{(\Delta_p-\Delta_{c1})+i\gamma_{cb}} - \frac{\Omega_{c1}^*\Omega_{c2} X_1}{(\Delta_p-\Delta_{c2})+i\gamma_{cb}} \times \frac{U_1}{1 - \frac{|\Omega_{c1}|^2|\Omega_{c2}|^2 T_1}{1-\cdots}}}.$$

The frequency of the reflected signal is $\omega_r = \omega_p - (\vec{k}_p - \vec{k}_r - 2\vec{k}_c)\cdot\vec{v} \approx \omega_p$, which is approximately equal to ω_p in the reflection direction according to the condition of phase matching. The process for the signal generation is as follows: The atoms transition from $|b\rangle$ to $|a\rangle$ by absorbing the probe field (photon) of frequency ω_p, then transition to $|c\rangle$ by emitting the copropagating field of ω_c, and then transition back to $|a\rangle$ by absorbing the counterpropagating coupling field of ω_c, and finally return to $|b\rangle$ by the emission of the reflected field. It can be represented by the factor $f^{[1]}(\Omega_{c1},\Omega_{c2})$, which depends only on the intensity of the coupling field (emitting and reabsorbing the same copropagating field and/or the same counterpropagating field). Note that the generated reflected light and the absorbed light in the backward field form a Doppler-free pair, and the absorbed probe photon and the increased photon in the forward field form another Doppler-free pair, because both pairs are at two photon resonances between $|b\rangle$ and $|c\rangle$ (or $|c\rangle$ and $|b\rangle$). This process also involves the absorption and emission of the same forward (or backward) coupling field (without net photon increase or reduction), indicated by $f^{[1]}(\Omega_{c1},\Omega_{c2})$. The emitted photon into the forward coupling field is neglected, because the initial intensity is more than 20 times stronger than that of the probe.

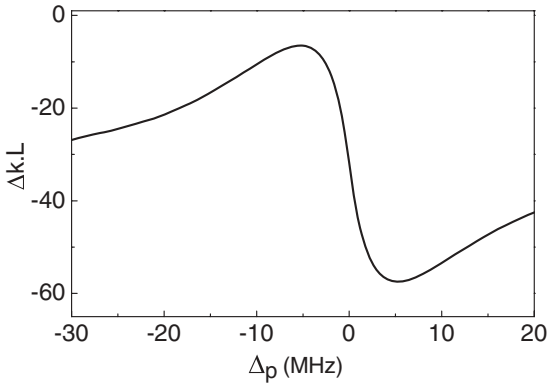

FIG. 6. Phase mismatching at $\theta = 0.14^\circ$ vs the probe detuning. The parameters are the same as in Fig. 5.

Now let us come back to the phase-matching condition, including the dispersion,

$$\Delta\vec{k} = \vec{k}_p - \vec{k}_r - 2\vec{k}_c = 0, \tag{11}$$

where $|\vec{k}_c| = n_c\omega_c/c$, $|\vec{k}_p| = n_p\omega_p/c$, and $|\vec{k}_r| = n_r\omega_r/c$. In our experimental scheme, energy conservation leads to equal frequencies of probe and reflected fields $\omega_p = \omega_e$, and $n_p = n_e = 1 + (1/2)\mathrm{Re}[3\pi N(\lambda_p/2\pi)^3(\gamma_{ab}/\Omega_p)\tilde{\rho}_{ab}^{[0]}]$ for both the probe and emission light are coupled to the same atomic transition. We set $n_c = 1$ for the dispersion and the absorption of the strong-coupling field can be neglected, the value of $\Delta\vec{k}$ is [see Fig. 1(b)]

$$\Delta k = 2(n_p\omega_p\cos\theta - \omega_c)/c = \big(2(\omega_p\cos\theta - \omega_c) + \mathrm{Re}\big[3\pi N(\lambda_p/2\pi)^3(\gamma_{ab}/\Omega_p)\tilde{\rho}_{ab}^{[0]}\big]\omega_p\cos\theta\big)/c. \tag{12}$$

At resonance $\omega_p = \omega_{ab}$, $\omega_c = \omega_{ac}$, the momentum could not be conserved for any angle θ, $\Delta k < 0$, because of $\omega_{ac} - \omega_{ab} = 2\pi \times 9.2$ GHz [see the energy level in Fig. 1(a)] and the second term on the right-hand of Eq. (11) is zero [representing the dispersion of the atoms; see Fig. 5(b)], consequently, the reflection signal is weak, as shown in Fig. 3. However, in Fig. 3 we observe that the reflected beam peaks at a probe detuning of $\Delta_p = 5$ MHz. It is well known that around the absorption peak, the gradient of the anomalous dispersion is very large [see Figs. 2(b) or 5(b)], that is to say, the value of the real part of $\tilde{\rho}_{ab}^{[0]}$ (the phase shift in experimental measurement results) changes sharply

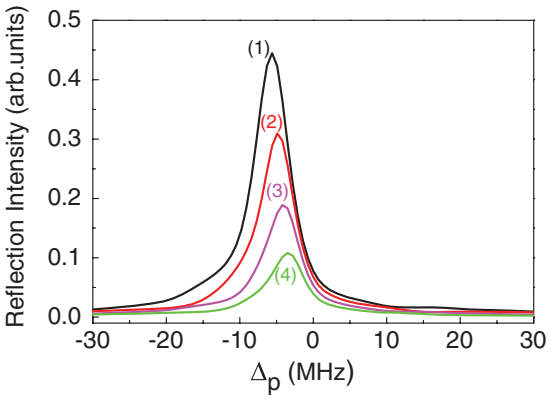

FIG. 7. (Color online) The numerical calculation for reflected signal vs probe detuning. Curve (1): $\theta = 0.14^\circ$ (black line); curve (2): $\theta = 0.24^\circ$ (red line); curve (3): $\theta = 0.34^\circ$ (magenta line); and curve (4): $\theta = 0.43^\circ$ (green line). The parameters are the same as those in Fig. 5.

with probe detuning. When the frequency ω_p decreases, the anomalous dispersion provides some compensation [represented by the term $\mathrm{Re}[3\pi N(\lambda_p/2\pi)^3(\gamma_{ab}/\Omega_p)\tilde{\rho}_{ab}^{[0]}]\omega_p \cos\theta/c$ in Eq. (12)] to the phase-matching condition. Note $\mathrm{Re}[3\pi N(\lambda_p/2\pi)^3(\gamma_{ab}/\Omega_p)\tilde{\rho}_{ab}^{[0]}] > 0$ for $\omega_p < \omega_{ab}$, which makes Eq. (11) closer to being satisfied, as is shown in Fig. 6, i.e., the phase mismatching ΔkL reaches a minimum at $\Delta_p \approx 5$ MHz and, consequently, we have a peak at $\omega_p < \omega_{ab}$. In Fig. 7 we plot the corresponding theoretical curves, which are close to the experimental curves in Fig. 3. The signal peaks are red detuned for $\sim$5 MHz because of the phase compensation induced from the anomalous dispersion (natural width of the excited state); see Figs. 3 or 7. For $\omega_p > \omega_{ab}$, we have $\mathrm{Re}[3\pi N(\lambda_p/2\pi)^3(\gamma_{ab}/\Omega_p)\tilde{\rho}_{ab}^{[0]}] < 0$, so that there is no phase compensation (in fact, it is even worse), and the reflected signal declines quickly. In the numerical calculation for the curves in Fig. 7, the summation over all atoms within the cell length is approximately replaced by an integration over the atoms within an effective distance $1/\beta$ and $\beta \propto \mathrm{Im}\rho_{ab}^{[0]}/\Omega_p$, as the probe field declines during the propagation, $I_p = I_{p0}e^{-\beta x}$.

IV. CONCLUSION

In conclusion, the reflection process, where the phase matching for the vacuum wave vectors (the geometric Bragg condition) cannot be fulfilled, is studied both theoretically and experimentally. The four waves involved are the copropagating and counterpropagating coupling fields, the probe, and the reflected field. The atoms absorb the probe and the counterpropagating coupling field, and meanwhile emit the copropagating coupling field and the reflected field. The probe and the copropagating coupling field form a Doppler-free pair, and the reflected and the counterpropagating coupling fields form another Doppler-free pair, so that we have Doppler-free reflection, because both pairs are at two-photon resonance. During the FWM process, the phase mismatching is compensated for by anomalous dispersion due to the strong absorption of the probe. When the frequency is redshifted from the resonance, we have a minimum phase mismatch and consequently a maximum of the reflection (a peak). The reflection is enhanced by strong anomalous dispersion, and more than 45% of reflection efficiency is observed. The efficiency increases with coupling power and the atom density. Here we would like to emphasize that FWM is different from the effect of third-order nonlinearity, because the atomic dipole depends on all orders of the coupling fields [see the $f^{[1]}(\Omega_{c1},\Omega_{c2})$ factor of Eq. (10)].

ACKNOWLEDGMENT

This work is supported in part by the NSFC (No. 10974126 and No. 60821004), the National Basic Research Program of China (No. 2010CB923102), the RGC of HK Government, and the FRG of HKBU.

[1] R. E. Slusher, L. W. Hollberg, B. Yurke, J. C. Mertz, and J. F. Valley, Phys. Rev. Lett. **55**, 2409 (1985).
[2] L. A. Wu, H. J. Kimble, J. L. Hall, and H. Wu, Phys. Rev. Lett. **57**, 2520 (1986).
[3] B. Dayan, A. S. Parkins, T. Aoki, E. P. Ostby, K. J. Vahala, and H. J. Kimble, Science **319**, 1062 (2008).
[4] A. Einstein, B. Podolsky, and N. Rosen, Phys. Rev. **47**, 777 (1935).
[5] S. L. Braunstein and P. van Loock, Rev. Mod. Phys. **77**, 513 (2005).
[6] A. Imamoğlu and S. E. Harris, Opt. Lett. **14**, 1344 (1989).
[7] C. Liu, Z. Dutton, C. H. Behroozi, and L. V. Hau, Nature (London) **409**, 490 (2001).
[8] D. F. Phillips, A. Fleischhauer, A. Mair, R. L. Walsworth, and M. D. Lukin, Phys. Rev. Lett. **86**, 783 (2001).
[9] H. Kang and Y. Zhu, Phys. Rev. Lett. **91**, 093601 (2003).
[10] M. D. Lukin, A. B. Matsko, M. Fleischhauer, and M. O. Scully, Phys. Rev. Lett. **82**, 1847 (1999).
[11] V. Boyer, A. M. Marino, R. C. Pooser, and P. D. Lett, Science **321**, 544 (2008).
[12] G. X. Li, H. T. Tan, and M. Macovei, Phys. Rev. A **76**, 053827 (2007).
[13] L. M. Duan, M. Lukin, J. I. Cirac, and P. Zoller, Nature (London) **414**, 413 (2001).
[14] K. J. Boller, A. Imamoğlu, and S. E. Harris, Phys. Rev. Lett. **66**, 2593 (1991).
[15] H. Schmidt and A. Imamoğlu, Opt. Lett. **21**, 1936 (1996).
[16] V. Boyer, C. F. McCormick, E. Arimondo, and P. D. Lett, Phys. Rev. Lett. **99**, 143601 (2007).
[17] L. Deng and M. G. Payne, Phys. Rev. Lett. **91**, 243902 (2003).
[18] H. Kang, G. Hernandez, and Y. Zhu, Phys. Rev. A **70**, 061804 (2004).
[19] S. Du, E. Oh, J. Wen, and M. H. Rubin, Phys. Rev. A **76**, 013803 (2007).
[20] C. Affolderbach, S. Knappe, R. Wynands, A. V. Taĭchenachev, and V. I. Yudin, Phys. Rev. A **65**, 043810 (2002).

[21] A. A. Zhukov, S. A. Zibrov, G. V. Romanov, Y. O. Dudin, V. V. Vassiliev, V. L. Velichansky, and V. P. Yakovlev, Phys. Rev. A **80**, 033830 (2009).
[22] A. M. Akulshin, S. Barreiro, and A. Lezama, Phys. Rev. Lett. **83**, 4277 (1999).
[23] H. Y. Ling, Y. Q. Li, and M. Xiao, Phys. Rev. A **57**, 1338 (1998).
[24] M. Bajcsy, A. S. Zibrov, and M. D. Lukin, Nature (London) **426**, 638 (2003).
[25] G. C. Cardoso, V. R. de Carvalho, S. S. Vianna, and J. W. R. Tabosa, Phys. Rev. A **59**, 1408 (1999).
[26] M. Mitsunaga and N. Imoto, Phys. Rev. A **59**, 4773 (1999).
[27] H. Kang, G. Hernandez, and Y. Zhu, J. Mod. Opt. **52**, 2391 (2005).
[28] H. P. Myers, *Introductory Solid State Physics* (Taylor & Francis, London, 2002).
[29] A. W. Brown and M. Xiao, Opt. Lett. **30**, 699 (2005).
[30] A.W. Brown and Min Xiao, J. Mod. Opt. **52**, 2365 (2005).
[31] I. Bae, H. Moon, M. Kim, L. Lee, and J. Kim, App. Opt. **47**, 4849 (2008).
[32] I. Bae, H. Moon, M. Kim, L. Lee, and J. Kim, Opt. Express **18**, 1389 (2010).